Bifurcation and stability analysis of static equilibrium configuration of curved pipe conveying fluid

Author(s):
Yan, Hao; Li, Mingwu; Wang, Lin

Publication date:
2023-01

Permanent link:
https://doi.org/https://doi.org/10.3929/ethz-b-000576149

Originally published in:
European Journal of Mechanics - A/Solids 97, https://doi.org/10.1016/j.euromechsol.2022.104813

European Journal of Mechanics / A Solids 97 (2023) 104813

Contents lists available at ScienceDirect

European Journal of Mechanics / A Solids

journal homepage: www.elsevier.com/locate/ejmsol

Bifurcation and stability analysis of static equilibrium configuration of curved pipe conveying fluid

Hao Yan [a,b], Mingwu Li [c,*], Lin Wang [a,b,**]

[a] Department of Engineering Mechanics, School of Aerospace Engineering, Huazhong University of Science and Technology, Wuhan, 430074, China
[b] Hubei Key Laboratory for Engineering Structural Analysis and Safety Assessment, Wuhan, 430074, China
[c] Institute for Mechanical Systems, ETH Zürich, Leonhardstrasse 21, 8092, Zürich, Switzerland

ARTICLE INFO

Keywords:
Curved pipe conveying fluid
Bifurcation
Absolute nodal coordinate formulation
Static equilibrium configuration

ABSTRACT

We present bifurcation and stability analysis of static equilibrium configurations of a clamped-clamped curved pipe conveying fluid in this paper. To capture large deformations of the pipe, this pipe is modeled with an absolute nodal coordinate formulation (ANCF). A technique of parameter continuation is used to solve the equilibria of the governing equation of this pipe system. Effects of external force, flow velocity and arc angle on the nonlinear responses of the curved pipe conveying fluid are discussed in detail. In the case of the curved pipe without any external loadings, the system admits two stable equilibria and an unstable equilibrium when the flow velocity exceeds a critical value on which a saddle-node bifurcation occurs. This critical flow velocity that characterizes the onset of the multistability is increased as the arc angle of the pipe increases. In addition, a pitchfork bifurcation occurs along the branch of the unstable equilibria. When the curved pipe is subjected to a concentrated force at its midpoint, the pipe deforms only in symmetrical mode shapes and undergoes a snap-through buckling under variations in the concentrated force. In contrast, when the curved pipe is subject to a gravity and the arc angle of the pipe exceeds a critical value, a pitchfork bifurcation buckling is observed under variations in the gravity. Along the secondary branch of this pitchfork bifurcation, equilibria in asymmetric mode shapes are found. Finally, effects of system parameters on these critical buckling loads are carefully explored.

1. Introduction

The dynamics of fluid-conveying pipes have attracted the attention of many researchers, partly because the broad applications of pipes in engineering systems, e.g. heat-exchangers, marine risers, oil pipelines, chemical plants and so on, and partly because the dynamical problem of pipes conveying fluid has become a paradigm in dynamics (Païdoussis and Li, 1993). An overview of studies on the dynamics of pipes conveying fluid can be found in the reviews by Païdoussis (1998) and Ibrahim (2010).

Numerous literatures of the dynamics of pipes conveying fluid have sprung up in the past several decades. Most of these published papers focused on straight pipes (Ghayesh et al., 2013; Guo et al., 2021; Païdoussis and Semler, 1993; Tang et al., 2022; Fan et al., 2022), while curved pipes have received relatively less attention due to the complication in theoretical modeling and dynamic analysis. Curved pipes in the shape of circular arcs are typical components in systems of pipelines. Therefore, the investigations on the dynamics and stability of curved pipes are necessary in order to reduce the vibrations of pipe systems and guarantee their stability.

Early studies (Chen, 1972a, 1972b, 1973; Doll and Mote, 1976; Hill and Davis, 1974) on the dynamics and stability of fluid-conveying curved pipes in the form of circular arcs have shown two opposing conclusions. Under an assumption that the centerline is inextensible, Chen (1972a, 1972b, 1973) derived the governing equations of a circular curved pipe by Newtonian and Hamiltonian formulations, and predicted that the curved pipe with two ends supported loses stability by divergence, i.e. buckling, as the internal flow velocity exceeds a certain critical value. However, Hill and Davis (1974) as well as Doll and Mote (1976) concluded that the curved pipe with two ends supported does not buckle even at very high flow velocities if the centerline of the pipe is allowed to be extensible.

* Corresponding author.
** Corresponding author. Department of Engineering Mechanics, School of Aerospace Engineering, Huazhong University of Science and Technology, Wuhan, 430074, China.
E-mail addresses: yanhaohust@126.com (H. Yan), mingwli@ethz.ch (M. Li), wanglindds@hust.edu.cn (L. Wang).

https://doi.org/10.1016/j.euromechsol.2022.104813
Received 13 July 2022; Received in revised form 15 September 2022; Accepted 19 September 2022
Available online 22 September 2022

In order to explain these opposing conclusions mentioned above, Misra et al. (1988a, b) re-examined the dynamics and stability of fluid-conveying curved pipes using a finite element method. By comparing essential differences between a curved pipe with inextensible and extensible centerlines, they confirmed that the curved pipe with two ends supported could not lose stability even for sufficiently high flow velocities, and pointed out that the results based on the pipe model with an extensible centerline are more reliable. However, Jung and Chung (2006) pointed out that the theoretical model of extensible curved pipes proposed by Misra et al. (1988a) was based on small-deformation assumption, which can lead to unreliable results of natural frequencies at high flow velocities, because the equations of motion were linearized around the equilibrium configuration predicted by linear governing equations. Thus, Jung and Chung (2006) further derived new nonlinear equilibrium equations and linearized their equations of motion around the nonlinear equilibrium configuration. Numerical results by Jung and Chung (2006) demonstrate that the equilibrium configuration solutions predicted by nonlinear governing equations are more accurate and reasonable than those based on linearized equations.

Taking geometric nonlinearity and an infinitesimal strain assumption into account, Dupuis and Rousselet (1992, 1993) established nonlinear equations of motion for fluid-conveying curved pipes. However, the infinitesimal strain assumption is only valid when the pipe's deformation is small. Since the deformation of curved pipes may be large at high flow velocities, Jung and Chung (2008) constructed a nonlinear model of curved pipes by adopting Lagrange nonlinear strain, and investigated the in-plane and out-plane natural frequencies of a semi-circular pipe conveying fluid using Galerkin method. Their research demonstrated, once again, that the curved pipe with both ends supported does not buckle even at sufficiently high flow velocities.

Recently, Łuczko and Czerwiński (2019) proposed a model describing three-dimensional motions of curved pipes with consideration of extensible theory and geometric nonlinearities. Twelve nonlinear ordinary differential equations were used to determine the static equilibrium configuration of the pipe, and six partial differential equations with coefficients depending on static solutions were utilized to govern the vibration of the pipe near the static solutions. Based on Galerkin method with B-spline functions, the effects of flow velocity on the natural frequencies and vibration modes of curved pipes in the shapes of planar arcs and spirals as well as spatial cylindrical and conical spirals were analyzed. Their results demonstrated that the effects of flow velocity on natural frequencies of curved pipes with different initial configurations are weak, and instability of these curved pipes is impossible. Then, Czerwiński and Łuczko (2021) conducted a continuation of the work (Łuczko and Czerwiński, 2019) by studying the nonlinear vibrations of arc-type curved pipes with two ends fixed. The effects of flow velocity on the natural frequencies of the pipes with different curvature as well as the nonlinear responses of curved pipes conveying pulsating fluid flow were investigated based on a modified version of their previous model (Łuczko and Czerwiński, 2019). They found that numerical results agree with the experiment data. Moreover, experimental and theoretical studies on the dynamics of curved pipes conveying pulsating fluid can be also found in several other works (Czerwiński and Łuczko, 2018; Łuczko and Czerwiński, 2017; Luo et al., 2016; Nakamura et al., 2009; Ni et al., 2013; Yamashita et al., 2010).

According to the studies mentioned above, the curved pipe with two ends supported were reported to have only one static equilibrium configuration at a given flow velocity. That is obviously different from the perfect straight pipe, in which multiple equilibria (two nontrivial equilibria and one trivial equilibrium) might emerge together via a pitchfork bifurcation (Païdoussis, 1998; also see Guo et al., 2022a and 2022b for composite straight pipes). Multiple equilibria can also be found in pipes with a slight geometric imperfection (Dehrouyeh-Semnani et al., 2017; Ye et al., 2021; Zhu et al., 2021) via a transcritical bifurcation or a perturbed pitchfork bifurcation. Thus, one may wonder that whether there is only one equilibrium at any given flow velocity for the curved pipe with two ends supported, and if there are undiscovered equilibria. Motivated by these questions, we investigate the bifurcations of equilibria of curved pipes in this paper.

Although the theoretical models for curved pipes conveying fluid mentioned above have been improved by adding several types of geometric nonlinearities, previous theoretical analysis of the curved pipe is limited to relatively small deformations. Due to this limitation, it is difficult to capture all possible multiple solutions of a fluid-conveying curved pipe system because some solutions may have really large deformations.

To remove the limitation of the small deformation assumption, theoretical/numerical models of curved pipe based on large deformation theory have been recently constructed using absolute nodal coordinate formulation (ANCF) (Shabana, 1996) and geometrically-exact beam theory (GEBT) (Bauchau, 2011). Zhou et al. (2021b) proposed a curved pipe model with the aid of ANCF and the extended Lagrange equations for a non-material volume (Irschik and Holl, 2002), and investigated the static equilibrium configuration and nonlinear dynamics of slightly curved cantilevered pipes conveying fluid. In their further study (Zhou et al., 2021a), the stability and dynamics of a fluid-conveying supported pipe with a small geometric imperfection were investigated based on the same curved pipe model in Ref. (Zhou et al., 2021b). Tang and Sweetman (2021) developed a geometrically-exact theory for pipes conveying fluid, which allows large displacements and overall rigid-body motions of the pipe. Based on this theory, they studied the natural frequencies of a semi-circular pipe with two ends fixed. However, they did not address the multi-solution problem of fluid-conveying curved pipes with both ends supported.

This study is a continuation of our previous works (Zhou et al., 2021a, 2021b), and aims at finding multiple equilibria of clamped-clamped curved pipes conveying fluid. The bifurcation and stability of these equilibria under the variations in various of system parameters are highlighted in this paper. Utilizing the model proposed in Ref (Zhou et al., 2021b). and applying a parameter continuation method, the effects of flow velocity, arc angle and external forces on the equilibria of the clamped-clamped pipes in a shape of circular arcs are studied in detail. The multistability of the curved pipes is observed and some interesting and important conclusions are drawn out.

2. Modeling of the dynamical system

The system under consideration, shown in Fig. 1, consists of a clamped–clamped fluid-conveying curved pipe with arc length L, arc angle θ, mass per unit length m, cross-sectional area A_p, flexural rigidity EI, and a flowing fluid of mass per unit length M, with constant relative velocity U. In the present study, some basic assumptions of the pipe and fluid are introduced: (1) the pipe is uniform and slender; (2) the pipe

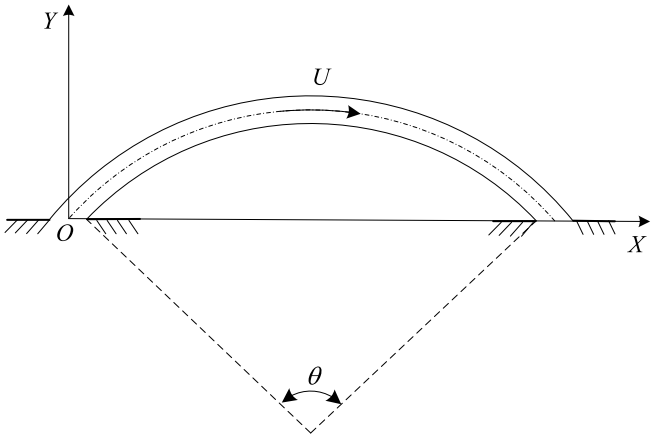

Fig. 1. Schematic of a curved pipe conveying fluid.

centreline is extensible; (3) the shear deformation and rotatory inertia are ignored; (4) the motion of pipe is planar; (5) the fluid is assumed to be incomprehensible and non-viscous.

A theoretical model based on an absolute nodal coordinate formulation (Shabana, 1996) and Lagrange's equations of motion for nonmaterial volumes (Irschik and Holl, 2002) was proposed in the work of Zhou et al. (2021b). This model enables the investigation of nonlinear dynamics of curved pipes conveying fluid that undergoes large displacements. According to Zhou et al. (2021b), the dynamic equation of a pipe element can be expressed in the following dimensionless form:

$$\mathbf{M}_e^*\ddot{\mathbf{q}}^* + \mathbf{C}_e^*\dot{\mathbf{q}}^* + \mathbf{K}_e^*\mathbf{q}^* + \mathbf{N}_e^*(\mathbf{q}^*) = \mathbf{F}_e^*, \tag{1}$$

where $\mathbf{q}^*$ is the dimensionless nodal coordinate vector, $\mathbf{M}_e^*$, $\mathbf{C}_e^*$, $\mathbf{K}_e^*$, $\mathbf{N}_e^*$ and $\mathbf{F}_e^*$ represent the mass matrix, damping matrix, stiffness matrix, nonlinear vector and external force of the pipe element, respectively. The expressions of these matrices are given by (Zhou et al., 2021b)

$$\mathbf{M}_e^* = \int_0^l \mathbf{S}^T\mathbf{S}\mathrm{d}x,$$

$$\mathbf{C}_e^* = u\sqrt{\beta}\int_0^l \frac{\mathbf{S}^T\mathbf{S}' - \mathbf{S}'^T\mathbf{S}}{\sqrt{\mathbf{q}_0^{*T}\mathbf{S}'^T\mathbf{S}'\mathbf{q}_0^*}}\mathrm{d}x + u\sqrt{\beta}L\left(\mathbf{S}^T\mathbf{S}|_{x=l} - \mathbf{S}^T\mathbf{S}|_{x=0}\right),$$

$$\mathbf{K}_e^* = -\left(u^2 + \frac{1}{2}\Pi\right)\int_0^l \frac{\mathbf{S}'^T\mathbf{S}'}{\mathbf{q}_0^{*T}\mathbf{S}'^T\mathbf{S}'\mathbf{q}_0^*}\mathrm{d}x + u^2L\left(\frac{\mathbf{S}^T\mathbf{S}'}{\sqrt{\mathbf{q}_0^{*T}\mathbf{S}'^T\mathbf{S}'\mathbf{q}_0^*}}|_{x=l} - \frac{\mathbf{S}^T\mathbf{S}'}{\sqrt{\mathbf{q}_0^{*T}\mathbf{S}'^T\mathbf{S}'\mathbf{q}_0^*}}|_{x=0}\right),$$

$$\mathbf{N}_e^*(\mathbf{e}) = \frac{1}{2}\Pi\int_0^l \frac{\mathbf{S}'^T\mathbf{S}'\mathbf{q}^*\mathbf{q}^{*T}\mathbf{S}'^T\mathbf{S}'\mathbf{q}^*}{\left(\mathbf{q}_0^{*T}\mathbf{S}'^T\mathbf{S}'\mathbf{q}_0^*\right)^2}\mathrm{d}x + \int_0^l\left(\frac{\left[\left(\widetilde{\mathbf{I}}\mathbf{S}'\right)^T\mathbf{S}'' + \mathbf{S}''^T\left(\widetilde{\mathbf{I}}\mathbf{S}'\right)\right]\mathbf{q}^*\mathbf{q}^{*T}\left(\widetilde{\mathbf{I}}\mathbf{S}'\right)^T\mathbf{S}''\mathbf{q}^*}{\left(\mathbf{q}^{*T}\mathbf{S}'^T\mathbf{S}'\mathbf{q}^*\right)^3} - \frac{3\mathbf{S}'^T\mathbf{S}'\mathbf{q}^*\mathbf{q}^{*T}\left(\widetilde{\mathbf{I}}\mathbf{S}'\right)^T\mathbf{S}''\mathbf{q}^*\mathbf{q}^{*T}\left(\widetilde{\mathbf{I}}\mathbf{S}'\right)^T\mathbf{S}''\mathbf{q}^*}{\left(\mathbf{q}^{*T}\mathbf{S}'^T\mathbf{S}'\mathbf{q}^*\right)^4}\right)\mathrm{d}x - \int_0^l \frac{\mathbf{q}_0^{*T}\left(\widetilde{\mathbf{I}}\mathbf{S}'\right)^T\mathbf{S}''\mathbf{q}_0^*}{\left(\mathbf{q}_0^{*T}\mathbf{S}'^T\mathbf{S}'\mathbf{q}_0^*\right)^{3/2}}\left(\frac{\left[\left(\widetilde{\mathbf{I}}\mathbf{S}'\right)^T\mathbf{S}'' + \mathbf{S}''^T\left(\widetilde{\mathbf{I}}\mathbf{S}'\right)\right]\mathbf{q}^*}{\left(\mathbf{q}^{*T}\mathbf{S}'^T\mathbf{S}'\mathbf{q}^*\right)^{3/2}} - \frac{3\mathbf{S}'^T\mathbf{S}'\mathbf{q}^*\mathbf{q}^{*T}\left(\widetilde{\mathbf{I}}\mathbf{S}'\right)^T\mathbf{S}''\mathbf{q}^*}{\left(\mathbf{q}^{*T}\mathbf{S}'^T\mathbf{S}'\mathbf{q}^*\right)^{5/2}}\right)\mathrm{d}x. \tag{2}$$

where $\mathbf{S}$ is the global shape function of the 2D gradient deflection ANCF element (Shabana, 1996), x is the arc-length coordinate of an arbitrary point on the pipe element in the undeformed configuration, l denotes the original length of the pipe element, the over-dot denotes the derivatives with respect to dimensionless time τ and the subscript "0" of $\mathbf{q}^*$ denotes the initial undeformed configuration. The superscripts "*" of notations above denotes variables in dimensionless form. Moreover, the matrix $\widetilde{\mathbf{I}}$ is given as follows:

$$\widetilde{\mathbf{I}} = \begin{bmatrix} 0 & -1 \\ 1 & 0 \end{bmatrix}. \tag{3}$$

In Eqs. (1) and (2), several dimensionless quantities and parameters are introduced. They are defined as below

$$\tau = \sqrt{\frac{EI}{M+m}}\frac{t}{L^2}, \quad \mathbf{q}^* = \frac{\mathbf{q}}{L}, \quad \mathbf{q}_0^* = \frac{\mathbf{q}_0}{L}, \quad u = \sqrt{\frac{M}{EI}}UL, \quad \beta = \frac{M}{M+m}, \quad \Pi = \frac{A_P L^2}{I}, \tag{4}$$

where $\mathbf{q}$ is the dimensional nodal coordinate vector of the pipe element; u denotes the dimensionless flow velocity; β is a mass ratio and Π is the coefficient related to the slenderness of the pipe.

After assembling the dynamic equation (Eq. (1)) of each pipe element, the equations of motion of this pipe system are obtained as follows:

$$\mathbf{M}\ddot{\mathbf{e}} + \mathbf{C}\dot{\mathbf{e}} + \mathbf{K}\mathbf{e} + \mathbf{N}(\mathbf{e}) = \mathbf{F}, \tag{5}$$

where $\mathbf{e}$, $\mathbf{M}$, $\mathbf{C}$, $\mathbf{K}$, $\mathbf{N}$ and $\mathbf{F}$ are the generalized nodal coordinates, mass matrix, damping matrix, stiffness matrix, vector of nonlinearities and external force vector for the whole pipe system.

3. Methods of solution

The main goal of this study is to investigate how the equilibria of the pipe system (5) are affected by system parameters. The number of the equilibria and the stabilities of these equilibria may be changed under the variations in system parameters. In other words, the dynamical system can undergo bifurcations in terms of equilibria. These bifurcations are important for understanding the multistability of the system and hence answer the questions that we asked in the introduction section.

Let $\mathbf{x} = (\mathbf{e}, \dot{\mathbf{e}})$, Eq. (5) can be rewritten as

$$\dot{\mathbf{x}} = \mathbf{f}(\mathbf{x}, p). \tag{6}$$

Here $p \in \mathbb{R}$ is control parameter, e.g., the flow speed or external load.

Equilibria of the pipe system are solved from

$$\mathbf{f}(\mathbf{x}, p) = 0. \tag{7}$$

For an obtained equilibrium $\mathbf{x}^*$ corresponding a given parameter p^*, the stability of this static configuration is determined from the spectrum of the Jacobian of the vector field with respect to the state $\mathbf{x}$, evaluated at $(\mathbf{x}^*, p^*)$. Let this spectrum be denoted by $\mathrm{Spect}(\mathbf{x}^*, p^*)$. We have

$$\mathrm{Spect}(\mathbf{x}^*, p^*) = \{\lambda : D_{\mathbf{x}}\mathbf{f}(\mathbf{x}^*, p^*)\mathbf{v} = \lambda\mathbf{v}\} \tag{8}$$

Provided that all elements of $\mathrm{Spect}(\mathbf{x}^*, p^*)$ have negative real parts, then $\mathbf{x}^*$ is stable. In contrast, if any of $\mathrm{Spect}(\mathbf{x}^*, p^*)$ has positive real part, $\mathbf{x}^*$ is unstable. We can further infer bifurcations of equilibria from their spectrum. For instance, if $\mathbf{x}^*$ is a saddle-node (SN) bifurcated equilibrium, then $\mathrm{Spect}(\mathbf{x}^*, p^*)$ includes a zero eigenvalue (Guckenheimer and Holmes, 2013); if $\mathbf{x}^*$ is a Hopf bifurcated equilibrium, then the spectrum $\mathrm{Spect}(\mathbf{x}^*, p^*)$ includes a pair of pure imaginary eigenvalues (Guckenheimer and Holmes, 2013).

Since the number of unknowns in Eq. (7) is more than the number of equations by one, we obtain a one-dimensional manifold of equilibria possibly along with some branch points (BPs). At a BP $(\mathbf{x}^*, p^*)$, several solution branches intersect with each other. In general, two branches intersect at the BP. Consequently, the rectangular Jacobian matrix $[D_{\mathbf{x}}\mathbf{f}(\mathbf{x}^*, p^*), D_p\mathbf{f}(\mathbf{x}^*, p^*)]$ has a two-dimensional null space. One can utilize this fact to detect and locate the BP (Kuznetsov et al., 1998). Along each solution branch, one can again infer the stability and bifurcation of equilibria on the branch from the spectrum of the equilibria.

Parameter continuation (Ahsan et al., 2022; Dankowicz and Schilder, 2013) provides a powerful tool to cover the solution manifold of the nonlinear system given by Eq. (7). It enables the detection of bifurcation points and the switch of branches at a BP where several solution branches pass through. Here we apply the parameter continuation implemented in COCO (Ahsan et al., 2022; Dankowicz and Schilder, 2013; Schilder et al., 2020) to obtain the solution manifold of the equilibria of the system defined by Eq. (6). COCO is a publicly available continuation package for computational nonlinear analysis and design. We will use the ep-toolbox of COCO to obtain solution branches of the equilibria of Eq. (6) under variations in certain system parameters. Along these solution branches, COCO determines the stability of a given equilibrium from the spectrum of the equilibrium and detects bifurcation points such as SN points and Hopf points (Guckenheimer and Holmes, 2013). It also detects BPs and support branch switching at a given BP. These capabilities of COCO make it very useful in finding bifurcation diagrams, which summarize the dynamical behavior of the system.

4. Results and discussions

In this section, the bifurcation and stability analysis of static equilibrium configurations of a clamped-clamped curved pipe conveying fluid will be explored. Since the dynamic characteristics of pipes with and without external forces have fundamental difference, the dynamics of pipes conveying fluid with and without external force will be treated separately.

Unless otherwise stated, several dimensionless parameters used in the following numerical calculations are fixed as $L = 1$, $\beta = 0.2$, $\Pi = 10{,}000$. Moreover, a damping force proportional to $\dot{\mathbf{e}}$ is added to Eq. (5) to take the effects of air damping into consideration. We set this damping coefficient to be 0.01. This added damping has no effects on the number of equilibria of Eq. (5) but can affect the stability of the obtained equilibria. The results presented in this section are robust with respect to the damping coefficient as long as it is small.

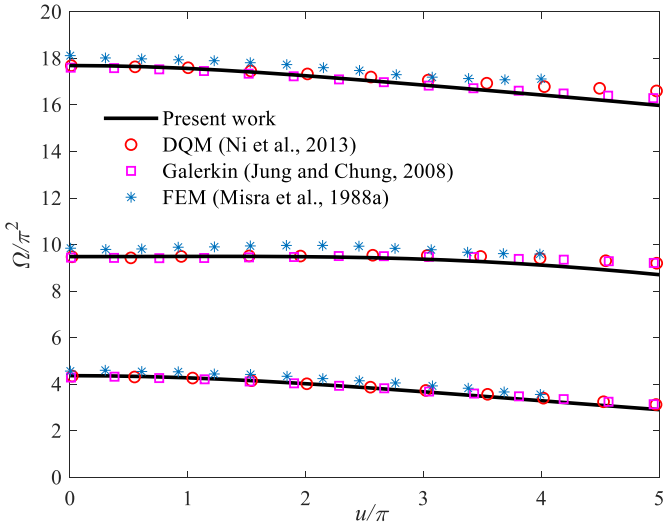

Fig. 2. Dimensionless natural frequencies Ω of a clamped-clamped semi-circular pipe conveying fluid as a function of dimensionless flow velocity u; for $\beta = 0.5$ and $\Pi = 10{,}000$.

Table 1
Dimensionless natural frequencies Ω for a clamped-clamped circular arch with different arc angles (θ).

θ	Mode	Exact solution	ANCF	Relative error (%)
90°	1	55.82526	55.8196	0.010%
	2	106.7298	106.1187	0.573%
	3	193.0367	192.9868	0.026%
120°	1	51.96933	51.9632	0.012%
	2	103.5759	103.2585	0.306%
	3	188.3600	188.2914	0.036%
150°	1	47.69263	47.6882	0.009%
	2	99.71315	99.5326	0.181%
	3	182.9127	182.8465	0.036%
180°	1	43.27261	43.2717	0.002%
	2	95.26019	95.1594	0.106%
	3	176.8814	176.8361	0.026%

Remark: For the exact solutions given by Tüfekçi and Arpaci (1998), the slenderness ratios R/i of the arch equals to 100.

In order to ensure the accuracy and computational efficiency of the numerical calculations, 20 pipe elements will be adopted. The convergence test can be found in Appendix A.

4.1. Validation of the ANCF procedure

We first validate the correctness of the present model based on the ANCF procedure. For such a purpose, the dimensionless natural frequencies of a clamped–clamped semi-circular pipe conveying fluid are calculated and compared with those in existing literature. Fig. 2 shows the evolutions of the lowest three natural frequencies with increasing flow velocity. In this figure, the solid lines, circles, rectangles and asterisks represent the frequencies solved by ANCF, differential-quadrature methods (DQM) (Ni et al., 2013), Galerkin methods (Jung and Chung, 2008) and finite-element methods (FEM) based on extensible theory (Misra et al., 1988a), respectively. As shown in Fig. 2, the present results are in good agreement with those reported in previous studies.

As an alternative validation, the curved ANCF pipe element should be degenerated into a curved beam element when the internal fluid flow is removed. To check this, the natural frequencies of a clamped-clamped circular arch with different arc angles are calculated and compared to exact solutions (Tüfekçi and Arpaci, 1998). Results listed in Table 1 show that the maximum relative error of dimensionless natural frequencies Ω obtained by the exact solutions and the ANCF procedure is about 0.573%. Therefore, the ANCF procedure used in this study is verified to be valid and reliable.

4.2. Pipes conveying fluid without external force

The nonlinear analysis of the pipe system without any external force is summarized in several bifurcation diagrams, in which, typically, the global position of the pipe's midpoint in the Y direction is plotted as a function of the flow velocity u. The bifurcation diagrams in each panel of Fig. 3 consists of three solution branches and special points such as the branch points (BP) of pitchfork type and saddle-nodes (SN). These solution branches are distinguished by blue, red and purple lines, respectively. In Fig. 3, the solid and dashed lines represent stable and unstable solutions, the BP and SN are denoted as green diamonds and red dots. Moreover, several typical static equilibrium configurations of the pipe along with solution branches are also displayed in the same color and line styles as the corresponding branches. It should be mentioned that the initial configurations of the pipe are shown in black lines, and the static equilibrium configurations of the pipe at the BPs and SNs are highlighted by bold red and green lines, respectively.

The results of a straight pipe with two ends clamped, shown in Fig. 3

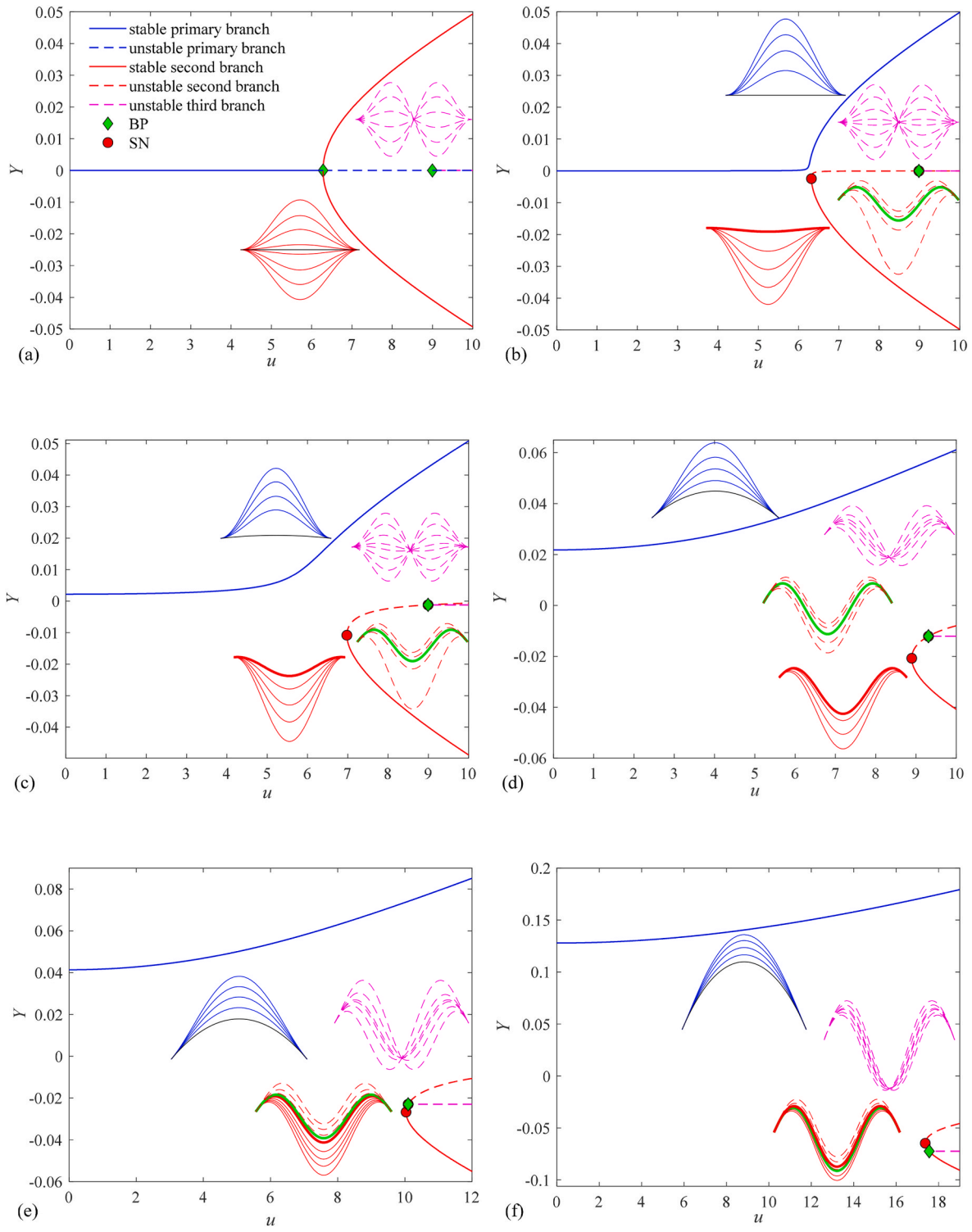

Fig. 3. Bifurcation diagrams and static equilibrium configurations of the straight pipe and curved pipe with different arc angles: (a) $\theta = 0^\circ$ (straight pipe); (b) $\theta = 0.01^\circ$; (c) $\theta = 1^\circ$; (d) $\theta = 10^\circ$; (e) $\theta = 19^\circ$; (f) $\theta = 60^\circ$. Here, and throughout the paper, the solid lines indicate stable solution branches, while the dashed lines mark unstable solution branches. The red circles denote saddle-node bifurcation points and the green diamonds denote branch points where two branches intersect. (For interpretation of the references to color in this figure legend, the reader is referred to the Web version of this article.)

(a), demonstrate that the pipe remains at the stable primary branch, i.e. the trivial equilibrium position, before losing stability by a pitchfork bifurcation (the onset of buckling) at $u = 6.28$ (BP1). Then, the system bifurcates from the stable primary branch to the stable second branch, which has two nontrivial symmetrical stable segments. The buckling amplitude of the pipe increases with increasing flow velocity. Moreover, in the post-buckling region, the trivial equilibrium in the primary branch is unstable, and the second pitchfork bifurcation point (BP2) is detected along this branch at $u = 8.99$. Then, an unstable third branch comes out from BP2. It is seen from sampled static configurations in Fig. 3(a) that the static configurations on the third branch (see the magenta dashed lines) are antisymmetric with respect to the midpoint and hence $Y =$

0 along this branch. This explains that the purple branch coincides with the main branch in Fig. 3(a). These results of the clamped-clamped straight pipe conveying fluid are consistent with that of Païdoussis (1998). One can also find that the static equilibrium configurations of the straight pipe on the second and third branches are in the first and second mode shapes, respectively. Although these unstable static equilibrium configurations cannot be found in experiments without control, their stable and unstable manifolds have great impact on the global dynamics of nonlinear systems (Guckenheimer and Holmes, 2013; Kuznetsov et al., 1998).

Next, we investigate how the bifurcation diagram is affected by the curvature of the curved pipe. For an arc-type curved pipe, arc angle θ equals to the curvature radius as the arc length L is 1 (cf. Figs. 1 and 8). Hence, several curved pipes with arc angle $\theta = 0.01^\circ$, 1°, 10°, 19°, 60° are considered for studying how the variation of curvature radius affects the dynamical behavior of the curved pipe. The main results are shown in Fig. 3(b–f).

The case of arc angle $\theta = 0.01^\circ$ can be viewed as a small imperfection or perturbation of a perfect straight pipe. Under the addition of this small perturbation, the first pitchfork bifurcation shown in Fig. 3(a) is destroyed and it is unfolded into a stable branch and an isolated saddle-node branch, i.e. the (blue) primary and (red) second branches shown in Fig. 3(b). Following bifurcation theories, this unfolding bifurcation phenomena can be detected for non-generic bifurcation, e.g. pitchfork bifurcation (Holmes and Marsden, 1978). By inspecting Fig. 3(b), the solutions on the primary branch start to deviate away from the initial configuration near $u = 6.3$. With the increase of flow velocity, the system undergoes a saddle-node (SN) bifurcation at $u = 6.317$ along the second branch. The second branch consists of an upper unstable part and a lower stable part that are connected via the SN point. Thus, this SN point marks the onset of multistability of the system for a given flow velocity.

On the upper unstable part of the second branch above, a pitchfork bifurcation appears at $u = 8.987$ and the unstable third branch comes out. Comparing Fig. 3(b) and (a), one can also find that the static equilibrium configurations of this slightly curved pipe on the stable primary, stable second or unstable third branches are very similar to that of the straight pipe. However, the static equilibrium configurations of this slightly curved pipe on the unstable part of the second branch exhibit a third-mode component of the pipe.

The bifurcation diagrams of Fig. 3(c–f) for $\theta = 1^\circ$, 10°, 19° and 60° show a similar feature to that for $\theta = 0.01^\circ$, namely a stable primary branch and an isolated second branch with a saddle node, as well as a third branch, which is generated by a pitchfork bifurcation. The flow velocities corresponding to the saddle node and the pitchfork bifurcation point are listed in Table 2. These results indicate that the flow velocities for SN and BP increase as the arc angle θ increases, implying that the onset of multistability requires a higher flow velocity for a bigger arc angle θ. Moreover, the isolated branches move far away from the primary branches as the arc angle θ increases.

From Fig. 3(b–f), one can also find that the static equilibrium configurations are in extensional modes along the primary branches, as also pointed out in some other studies (Jung and Chung, 2006; Misra et al., 1988a; Yun-dong and Ze-gang, 2021; Zhou et al., 2021a). However, the solutions of the pipe system on the isolated branches were likely to be missed in some previous research studies (Jung and Chung, 2006; Misra et al., 1988a; Yun-dong and Ze-gang, 2021; Zhou et al., 2021a). Since the convergence to the isolated branches is strongly dependent on the initial conditions, these solutions can only be observed from forward simulation by setting initial conditions near to these isolated branches.

Thus, we can conclude that, beyond the critical flow velocity corresponding to the SN point, the curved pipe may have two stable static configurations: one in the primary branch and one in the stable part of the second branch which is isolated from the primary branch. It follows that the extensional mode on the primary branch is not globally stable. With suitable initial conditions, the pipe can approach to the stable configuration on the second branch in a steady state. We leave the identification of the basins of attraction for these two stable solutions to future studies.

The observed multistability can be easily validated by numerical integration. Indeed, we can apply proper perturbation to an obtained static configuration and then perform forward simulation. We can verify the stability of the static configuration based on the time history from the forward simulation. As an illustration of this verification, we verify the obtained static configurations for $u = 8$ in Appendix B.

Table 2
Dimensionless flow velocity u at SN and BP of the pipe system discussed in Fig. 3

θ	u	
	SN	BP
Straight pipe	–	6.285/8.996
0.01°	6.317	8.987
1°	6.978	8.990
10°	8.893	9.306
19°	10.03	10.1
60°	17.38	17.56

4.3. Curved pipes conveying fluid with external force

In this subsection, a fluid-conveying curved pipe with external force is considered by introducing a concentrated force F at the pipe's midpoint or a distributed force, i.e., a gravity load, as shown in Fig. 4. The nonlinear responses of the pipe with external forces can be analyzed through load-deflection diagrams. In the following analysis, the relations between deflections of the midpoint of the pipe in the X and Y directions, denoted as ΔX and ΔY, and non-dimensional concentrated force $P = FL^2/EI$or gravity load $\gamma = (M+m)gL^3/EI$ are discussed in detail.

4.3.1. Nonlinear responses of a semi-circular pipe

Consider a clamped-clamped semi-circular pipe conveying fluid with flow velocity $u = 10$. Two loading cases, i.e., Case I: the pipe with a concentrated force P, and Case II: the pipe with a gravity load γ, are considered for the investigation of the nonlinear responses of the pipe with external forces. The load-deflection diagrams shown in Fig. 5 are presented in a similar way to the bifurcation diagrams in Fig. 3. In particular, bifurcation curves along with sampled static configurations are presented.

The load-deflection diagram for Case I is shown in Fig. 5(a), which presents the relation between the deflection ΔY of the midpoint of the pipe and the concentrated force P. Inspecting Fig. 5(a), one can find that the pipe deforms along the primary branch and experiences a snap-through buckling at two limit points (also called fold points), i.e. the point of local extrema on the branch. Specifically, as P reaches 102.3 or 41.63, the pipe can suddenly buckle from the limit point A or C to the remote point B or D, respectively. In this case, the limit points are coincident with saddle-nodes or turning points where stable and unstable equilibria merge. Moreover, the static equilibrium configurations on the primary branches are found to be in a symmetrical mode shapes, as seen in Fig. 5(a).

The load-deflection diagram for Case II is shown in Fig. 5(b–c). Different from Case I, a pitchfork bifurcation and resulting second branch are observed in Case II, as seen in Fig. 5(b–c). The relation between deflection ΔY and gravity load γ shown in Fig. 5(b) demonstrates that the pipe deforms along the stable primary branch in a symmetrical mode shape until point A, where $\gamma = 254.8$ and a pitchfork bifurcation occurs. A secondary branch comes out at this pitchfork point. Then, the pipe deforms along the stable second branch in an asymmetric mode shape until the saddle-node (limit point) A', where $\gamma = 255.8$ and a snap-through buckling occurs. Also, at $\gamma = 64.17$, the pipe can snap back from the saddle-node (limit point) C to point D. Since the limit point A'' is located on the unstable primary branch, the pipe cannot buckle via the

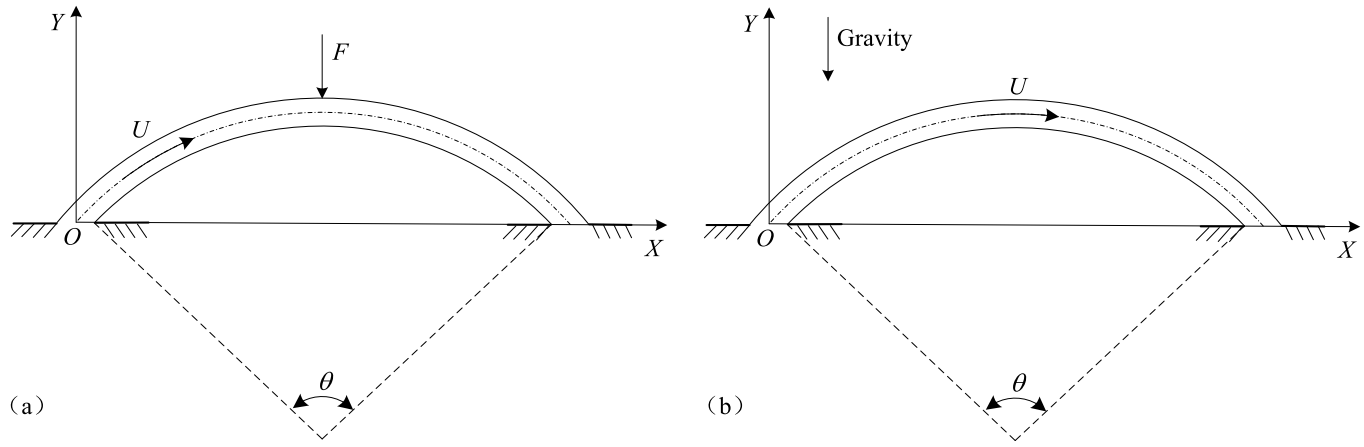

Fig. 4. Schematic of a curved pipe conveying fluid with (a) a concentrated force F at its midpoint and (b) a gravity load.

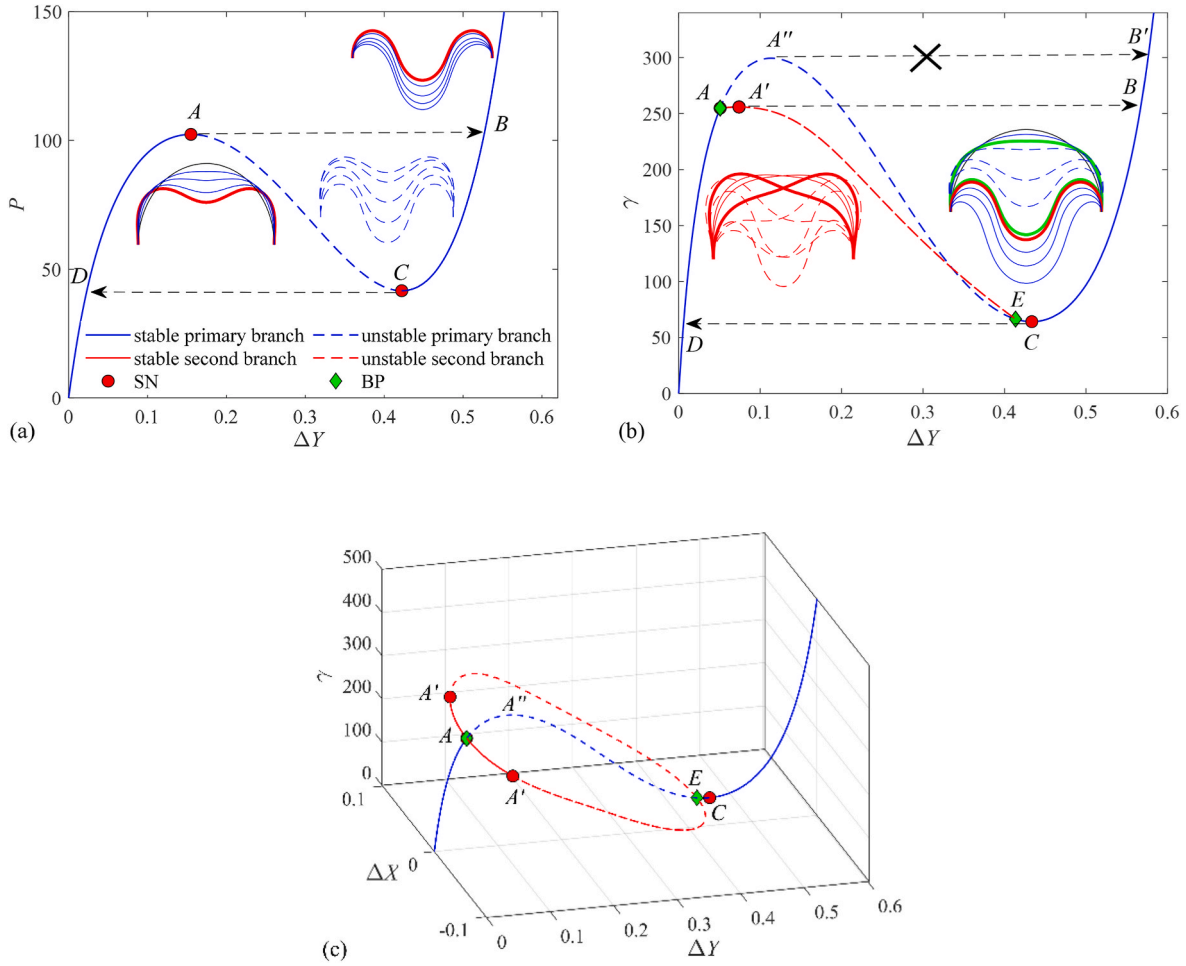

Fig. 5. Load-deflection diagrams and static equilibrium configurations of a clamped-clamped semi-circular pipe conveying fluid as $u = 10$: (a) in the plane (P, ΔY); (b) in the plane (γ, ΔY); (c) in the space (γ, ΔY, ΔX). (Color figure online)

path $A''B'$. We note that the second branch actually has two segments, and they form a loop that is symmetric about the plane $\Delta X = 0$ (see Fig. 5 (c)). Therefore, these two segments are coincided and collapsed into a single segment in Fig. 5(b). Since there are a pair of equilibria for each given γ on the second branch (see the red lines in Fig. 5(c)), the pipe can deform into two asymmetric mode shapes when the gravity load is between critical loads corresponding to branch points A and E.

It is interesting to investigate the effect of flow velocity on the nonlinear responses of the conveying-fluid pipe with external forces. Loading cases I and II are considered again for the clamped-clamped semi-circular pipe conveying fluid as the flow velocity varies from 1 to 10. It can be seen from Fig. 6(a) and (b) that the load-deflection curves for $u \in [1, 10]$ are very similar to each other. To obtain a deeper understanding of the effects of flow velocity on the pipe's behavior, special points (SN and BP) on the load-deflection curves are extracted and

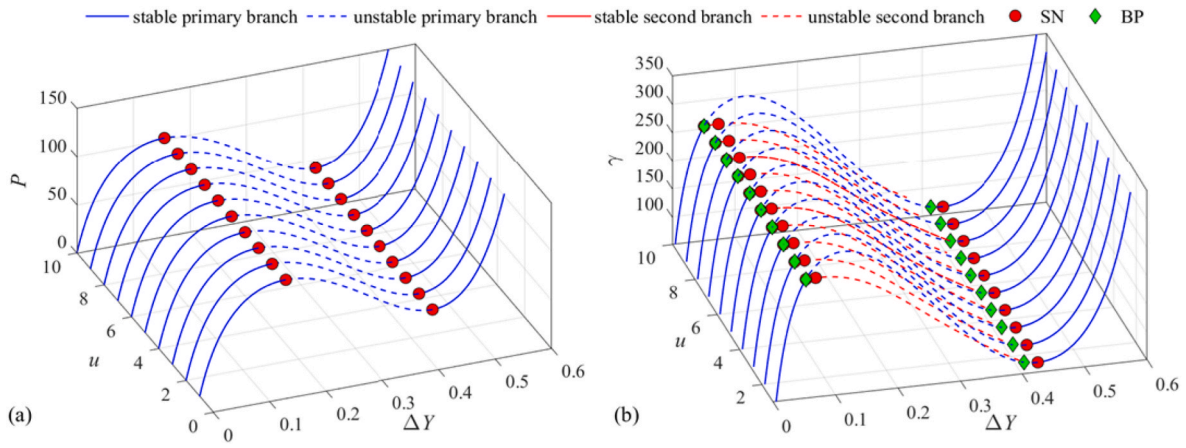

Fig. 6. Load-deflection diagrams of a clamped–clamped semi-circular pipe with (a) concentrated force P and (b) a gravity load γ, for different flow velocities. (Color figure online)

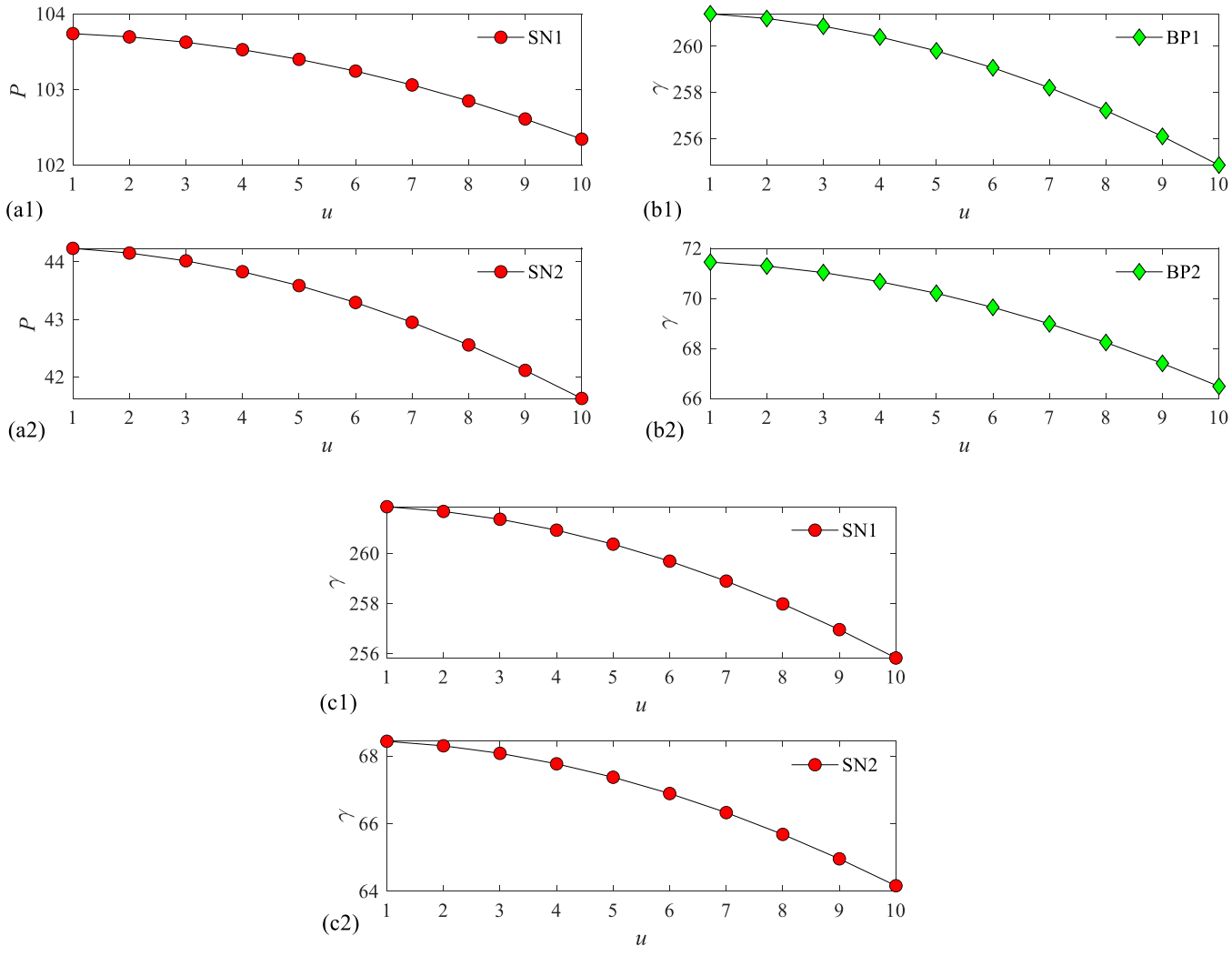

Fig. 7. The effects of flow velocity on the special points extracted from Fig. 6: (a1) SN1 and (a2) SN2 for case I; (b1) BP1 and (b2) BP2 for case II; (c1) SN1 and (c2) SN2 for case II. Numbers 1 and 2 after SN and BP indicate the order of the special points in the positive direction of ΔY-axis.

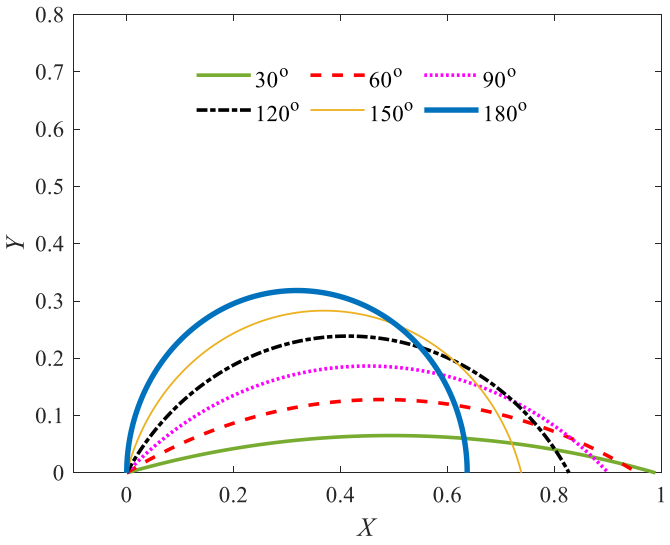

Fig. 8. Schematic of an arc-type curved pipe with different arc angles. Note that the arc length of the pipe is fixed to be $L = 1$. (Color figure online)

plotted in Fig. 7, from which one can find that the value of P and γ for these special points are decreased slightly with increasing u.

Thus, one can conclude that the load-deflection diagrams of the semi-circular pipe are insensitive to the variations in flow velocity.

4.3.2. *Nonlinear responses of an arc-type curved pipe*

To study the effect of arc angle θ on the nonlinear responses of curved pipes, several typical arc-type curved pipes with $\theta = 30°$, $60°$, $90°$, $120°$, $150°$ and $180°$ are considered (see Fig. 8). The arc-type curved pipes shown in Fig. 8 have the same arc length $L = 1$. Thus, the radius of each pipe can be defined as L/θ and changes with the variation of θ.

The relations between the load and the deflection for different clamped-clamped arc-type curved pipes with $u = 5$ for different external forces are illustrated in Fig. 9.

For the case of pipes with a concentrated force, it can be seen from Fig. 9(a) that the nonlinear responses of the arc-type curved pipes are similar to that of the semi-circular pipe discussed in Section 4.3.1. One can also find that the saddle nodes, i.e., the limit points, rise along the P-axis as θ varies from $30°$ to $180°$. This means that increasing the arc angle can raise the critical value of P.

For the case of pipes with a gravity load, it can be seen from Fig. 9(b) that the nonlinear responses of the arc-type curved pipes are different from that of a semi-circular pipe. The pipe with $\theta = 30°$ can only deform along the primary branch (corresponding to symmetric static equilibrium configurations) and experience a snap-through buckling after the saddle node (coincided with the limit point). However, for the pipe with $\theta = 60°$, $90°$, $120°$ or $150°$, a pitchfork bifurcation occurs before the limit point (fold point) on the primary branch, and a second branch (corresponding to asymmetric static equilibrium configurations) comes out from the bifurcation. It should be noted that the solutions on the second branch are all unstable. However, stable solutions can be observed on the second branch when $\theta = 180°$, i.e., in the case of a semi-circular pipe. Thus, one can conclude that the pipe under a gravity load can only deform in symmetrical mode shapes when θ below a critical value, which is found to be about $175°$ in this study, and asymmetric static equilibrium configurations can be physically found for the pipe when θ exceeds this critical value.

The critical buckling load, defined as the onset value of the external load where the system has no stable static configuration, is an important measure for the buckling resistance of an arc-type curved pipe with external force. For the pipe with a concentrated force P, the critical buckling load is obtained from a saddle node on the primary branch. For the pipe with a gravity load, the critical buckling load can be inferred from a saddle-node bifurcation or a pitchfork bifurcation, depending on whether stable solutions can be found on the secondary branch born out of the pitchfork bifurcation. Specifically, we have the following three cases:

- (i) No pitchfork bifurcation is observed. The critical load is obtained from a saddle-node bifurcation on the primary branch, as seen in the cases of the pipes subject to a concentrated force P and also the case of the pipe under a gravity load with $\theta = 30°$.
- (ii) A pitchfork bifurcation is observed but there are no stable solutions on the secondary branch born out of the bifurcation. The critical buckling load is obtained from the pitchfork bifurcation point. This is the case of $\theta = 60°$, $90°$, $120°$ and $150°$ for the pipe subject to a gravity load.
- (iii) A pitchfork bifurcation is observed, and the secondary branch born out of the bifurcation consists of both stable and unstable segments that are connected via a saddle-node bifurcation. The critical buckling load is obtained from the saddle-node bifurcation on the second branch. This is the case of $\theta = 180°$ for the pipe subject to a gravity.

In order to show the effects of u and θ on the nonlinear responses of the pipe system more carefully, the critical buckling loads discussed above as functions of plane (θ, u) are shown as contour plots in Fig. 10. Inspecting Fig. 10, one can find that the critical buckling loads P and γ increase with the increase of θ. However, it can be seen from Figs. 10 and

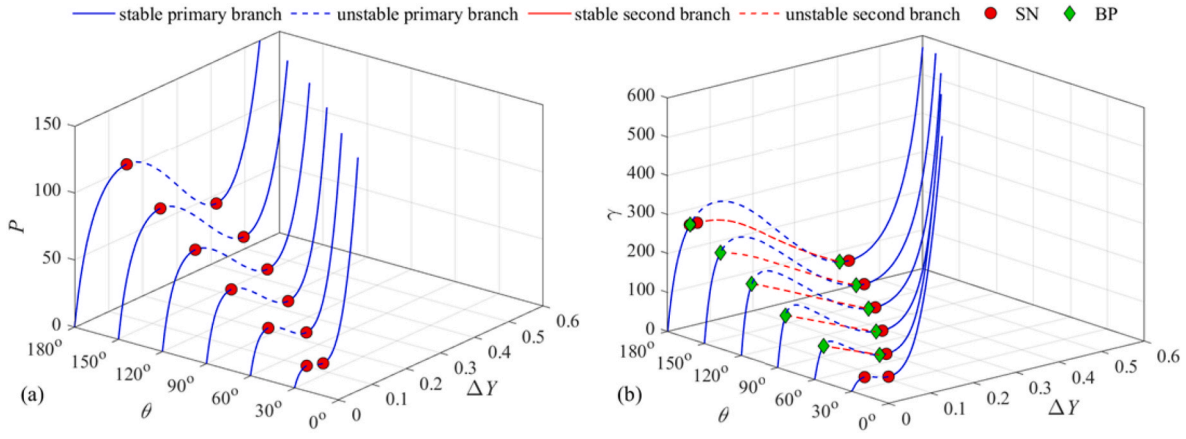

Fig. 9. Load-deflection diagrams of clamped-clamped arc-type pipe with (a) a concentrated force P and (b) a gravity load γ, for $u = 5$ and different θ. (Color figure online)

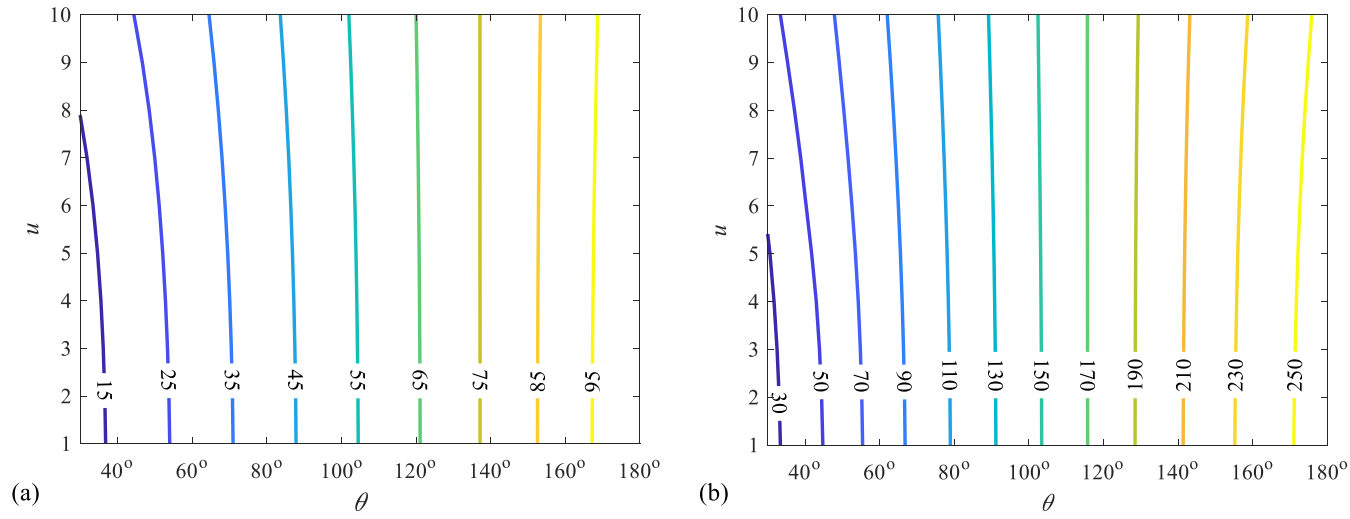

Fig. 10. Contour maps of the critical buckling load in the (θ, u) plane: (a) the pipe with a concentrated force P; (b) the pipe with a gravity load γ. (Color figure online)

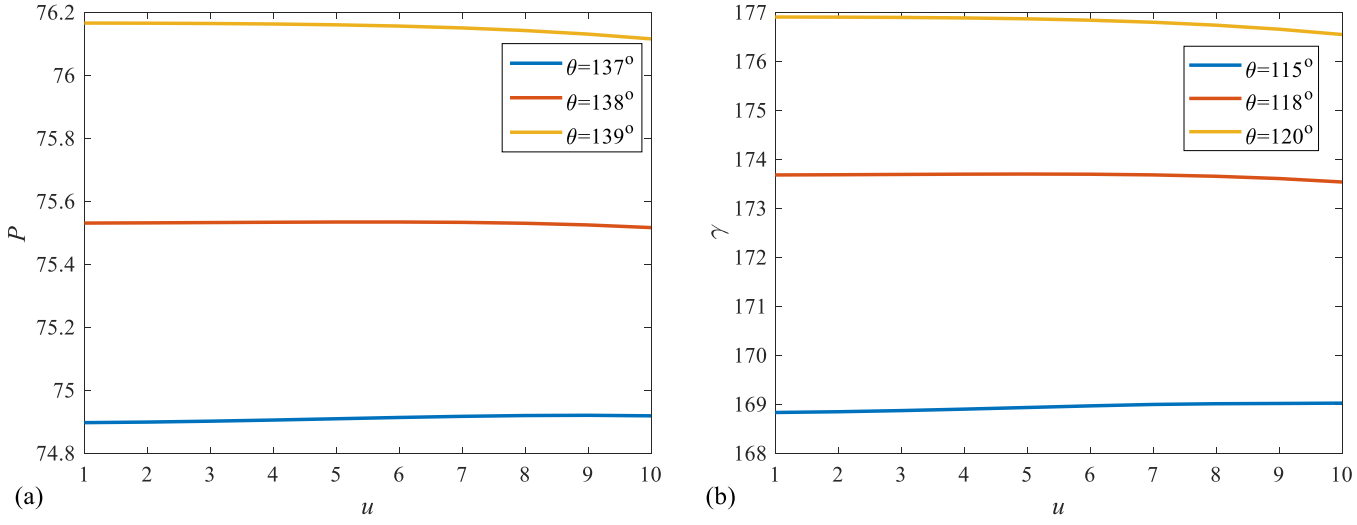

Fig. 11. Critical buckling loads as functions of flow velocity u: (a) the pipe with a concentrated force P; (b) the pipe with a gravity load γ. (Color figure online)

11 that the critical buckling loads P and γ increase with increasing u as θ is below a certain critical value, and decrease with increasing u as θ is above this critical value. In this study, the critical values of θ are about 138° and 118°.

Moreover, one can find that the effect of u on the critical buckling load weakens with increasing θ. This explains why the effects of flow velocity on the nonlinear responses of a clamped-clamped semi-circular pipe with external force are so weak.

5. Conclusion

This paper presents a study on the nonlinear responses of a clamped-clamped curved pipe conveying fluid. The nonlinear governing equation of the fluid-conveying curved pipe is given by the absolute nodal coordinate formulation and the extended Lagrange's equations for nonmaterial volumes. Based on the parameter continuation technique implemented in COCO, the bifurcation and stability of the static equilibrium configurations of the pipe are analyzed. The effects of external force, flow velocity and arc angle on the nonlinear responses of the pipe are discussed elaborately.

According to the numerical results, the following conclusions can be drawn for clamped-clamped pipes without external force:

(1) For an initially straight pipe, the pipe can buckle through a pitchfork bifurcation. However, as the initial configuration of the pipe becomes slightly curved, the pitchfork bifurcation of the pipe is destroyed and unfolded into a simple stable primary branch and an isolated saddle-node branch. Thus, the curved pipe can buckle through a saddle-node bifurcation at a critical flow velocity u for the bifurcation, which results in a new branch of stable equilibria. In other words, the curved pipe has two different stable static equilibrium configurations for each given u, provided the flow velocity is beyond the critical value for the saddle node bifurcation. Thus, the saddle-node marks the onset of multistability of the curved pipe system.
(2) The characteristics of the nonlinear responses of curved pipes are qualitatively similar as the arc angle varies. As the arc angle increases, the critical flow velocity for the saddle-node increases, and the isolated saddle-node branch moves away from the

primary branch. Thus, the onset of multistability requires a higher flow velocity for a bigger arc angle θ.

When the clamped-clamped fluid-conveying pipe is subjected to an external force, the following conclusions can be drawn:

(1) In the case of a curved pipe subjected to a concentrated force at its midpoint, the nonlinear responses of the pipe with different arc angles are simple and similar, i.e., the pipe can only deform along the primary branch in a symmetrical mode shape and experience a snap-through buckling at a saddle-node point.
(2) In the case of a curved pipe under a gravity load, the snap-through behavior of the pipe may be roughly classified into three different types as the arc angle varies. i) No pitchfork bifurcation is observed and the snap-through buckling of the pipe occurs at a saddle-node; ii) A pitchfork bifurcation is observed but there are no stable solutions on the secondary branch, and the pipe undergoes a snap-through buckling at the pitchfork bifurcation point; iii) A pitchfork bifurcation is observed and the secondary branch consists of both stable and unstable segments that are connected via saddle-node bifurcation, and the pipe undergoes a snap-through buckling at the saddle-node on the secondary branch. These three types of nonlinear responses of the curved pipe can be observed sequentially with increasing θ. In the first two types, only symmetric stable static equilibrium configurations are observed. However, both symmetric and asymmetric stable static equilibrium configurations occur in the third type.
(3) The critical buckling loads are affected by the flow velocity and the arc angle. Specifically, the critical buckling loads increases with increasing u as θ is below a certain critical value, and decreases with increasing u as θ is above this critical value. Increasing the arc angle can significantly raise the critical buckling load. Moreover, the effect of flow velocity on the critical buckling load becomes insignificant as the arc angle increases.

Author statements

Hao Yan: Conceptualization, Methodology, Software, Visualization, Writing-Original Draft, Funding acquisition. Mingwu Li: Conceptualization, Methodology, Software, Writing - Review & Editing. Lin Wang: Conceptualization, Supervision, Writing-Review & Editing, Funding acquisition.

Declaration of competing interest

The authors declare that they have no known competing financial interests or personal relationships that could have appeared to influence the work reported in this paper.

Data availability

Data will be made available on request.

Acknowledgement

The authors gratefully acknowledge the support of the National Natural Science Foundation of China (Nos. 12102139, 12072119 and 11972167).

Appendix A. Convergence tests

In order to obtain reliable numerical results, a proper number N of pipe elements should be determined by a convergence test. Consider the same pipe system discussed in subsection 4.3.1, the special points (saddle node and bifurcation point) on the load-deflection curves of pipe system corresponding to different N are obtained and shown in Fig. A1. Inspecting Fig. A1, one can find that converged results can be obtained as N exceeds 18. Thus, N = 20 is a suitable choice with the consideration of accuracy and efficiency.

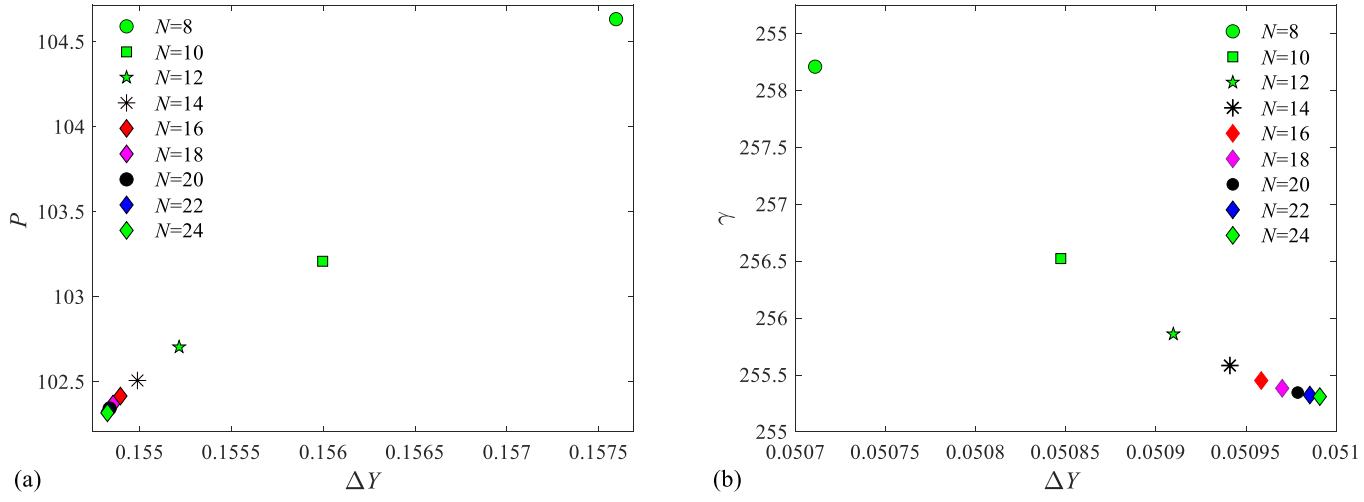

Fig. A1. Location of the special points on the load-deflection curves under different numbers of pipe elements N: (a) the first saddle node in Fig. 5(a); (b) the first branch point in Fig. 5(b). Note that the points of $N = 20$, 22 and 24 in figure (a) almost coincide with each other. In figure (b), the max absolute relative errors of (γ, ΔY) at points of $N = 20$ and 22 with respect to point of $N = 24$ are about 0.1962‰ and 0.1961‰. (Color figure online)

Appendix B. Validation of the multistability

In this appendix, we validate the observed multistability of static configurations in Fig. 3(c) using numerical integration. For the purpose of illustration, we focus on the case that the flow velocity $u = 8$. We have three coexisting static configurations at this flow velocity: one stable configuration on the primary branch (see the blue branch in Fig. 3(c)), one stable and one unstable configuration on the secondary branch that

detached from the primary branch (cf. The red branch in Fig. 3(c)). We will apply small perturbations to these configurations, perform forward simulations with the perturbed states as initial conditions, and verify the three configurations (and their stability types) using the time histories of these forward simulations.

We plot the time histories of the forward simulations in Fig. B1. Here the forward simulations are conducted via Runge-Kutta methods. In panel (a), a small perturbation, 0.01, at the pipe's midpoint along Y direction, is applied to the obtained static configuration on the stable primary branch. This perturbed trajectory converges to the stable configuration predicted by COCO, which validates the stable configuration on the primary branch.

In panel (b), a same perturbation is applied to the obtained stable configuration on the secondary branch. From the time history, we see that the trajectory from numerical integration converges to a static configuration, which is the same as the stable configuration obtained from COCO. Therefore, the curved pipe indeed has two coexisting stable static configurations. Depending on the initial condition, this curved pipe can be buckled both upward and downward.

Now we validate the obtained unstable static configuration on the secondary branch. When a small perturbation is applied to this configuration, the perturbated state will converge to one of the two stable configurations that we discussed above. Indeed, when we apply the same perturbation (0.01 at the pipe's midpoint along Y direction) to the unstable static configuration, the system converges to the stable configuration on the primary branch, as seen in Fig. B1(c) (cf. Fig. B1(a)). We flip the direction of the small perturbation. Then it converges to the stable configuration on the secondary branch, as seen in Fig. B1(d) (cf. Fig. B1(b)). Consequently, we have validated the multistability using numerical integration.

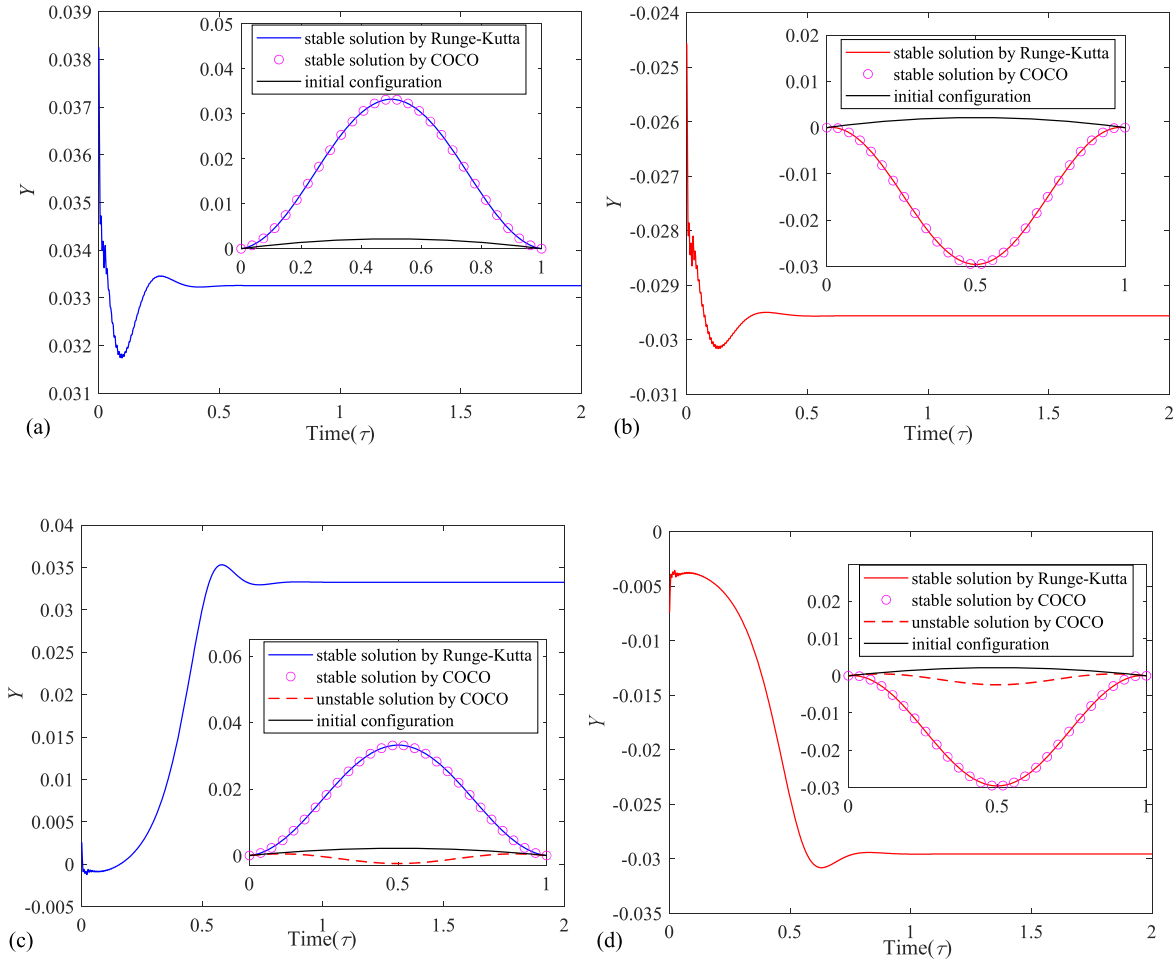

Fig. B1. Time histories of the deformed position of the pipe's midpoint in Y direction and corresponding static equilibrium configurations in steady states at $u = 8$ under different initial conditions. Here the initial (undeformed) configuration of the pipe (black line) is provided for reference. In the inlet of each panel, the configuration in steady state of numerical integration along with the solution obtained using COCO are plotted. (Color figure online)

References

Ahsan, Z., Dankowicz, H., Li, M., Sieber, J., 2022. Methods of continuation and their implementation in the COCO software platform with application to delay differential equations. Nonlinear Dynam. 107, 3181–3243.

Bauchau, O.A., 2011. Flexible Multibody Dynamics. Springer.

Chen, S.s., 1972a. Flow-induced in-plane instabilities of curved pipes. Nucl. Eng. Des. 23, 29–38.

Chen, S.s., 1972b. Vibration and stability of a uniformly curved tube conveying fluid. J. Acoust. Soc. Am. 51, 223–232.

Chen, S.s., 1973. Out-of-Plane vibration and stability of curved tubes conveying fluid. J. Appl. Mech. 40, 362–368.

Czerwiński, A., Łuczko, J., 2018. Non-planar vibrations of slightly curved pipes conveying fluid in simple and combination parametric resonances. J. Sound Vib. 413, 270–290.

Czerwiński, A., Łuczko, J., 2021. Nonlinear vibrations of planar curved pipes conveying fluid. J. Sound Vib. 501, 116054.

Dankowicz, H., Schilder, F., 2013. Recipes for Continuation. Society for Industrial and Applied Mathematicsv.

Dehrouyeh-Semnani, A.M., Nikkhah-Bahrami, M., Yazdi, M.R.H., 2017. On nonlinear stability of fluid-conveying imperfect micropipes. Int. J. Eng. Sci. 120, 254–271.

Doll, R.W., Mote Jr., C.D., 1976. On the dynamic analysis of curved and twisted cylinders transporting fluids. J. Pressure Vessel Technol. 98, 143–150.

Dupuis, C., Rousselet, J., 1992. The equations of motion of curved pipes conveying fluid. J. Sound Vib. 153, 473–489.

Dupuis, C., Rousselet, J., 1993. Hamilton's principle and the governing equations of fluid-conveying curved pipes. J. Sound Vib. 160, 172–174.
Fan, X., Wu, N., Liu, Y., Guo, Q., 2022. Resonance system reliability and sensitivity analysis method for axially FGM pipes conveying fluid with adaptive kriging model. Acta Mech. Solida Sin. 1–9. https://doi.org/10.1007/s10338-022-00333-4.
Ghayesh, M.H., Païdoussis, M.P., Amabili, M., 2013. Nonlinear dynamics of cantilevered extensible pipes conveying fluid. J. Sound Vib. 332, 6405–6418.
Guckenheimer, J., Holmes, P., 2013. Nonlinear Oscillations, Dynamical Systems, and Bifurcations of Vector Fields. Springer Science & Business Media.
Guo, Q., Liu, Y., Chen, B., Zhao, Y., 2021. An efficient stochastic natural frequency analysis method for axially varying functionally graded material pipe conveying fluid. Eur. J. Mech. Solid. 86, 104155.
Guo, Y., Zhu, B., Li, Y., 2022a. Nonlinear dynamics of fluid-conveying composite pipes subjected to time-varying axial tension in sub- and super-critical regimes. Appl. Math. Model. 101, 632–653.
Guo, Y., Zhu, B., Yang, B., Li, Y., 2022b. Flow-induced buckling and post-buckling vibration characteristics of composite pipes in thermal environment. Ocean Eng. 243, 110267.
Hill, J.L., Davis, C.G., 1974. The effect of initial forces on the hydroelastic vibration and stability of planar curved tubes. J. Appl. Mech. 41, 355–359.
Holmes, P., Marsden, J., 1978. Bifurcation to divergence and flutter in flow-induced oscillations: an infinite dimensional analysis. Automatica 14, 367–384.
Ibrahim, R.A., 2010. Overview of mechanics of pipes conveying fluids—Part I: fundamental studies. J. Pressure Vessel Technol. 132, 034001.
Irschik, H., Holl, H.J., 2002. The equations of Lagrange written for a non-material volume. Acta Mech. 153, 231–248.
Jung, D., Chung, J., 2006. A steady-state equilibrium configuration in the dynamic analysis of a curved pipe conveying fluid. J. Sound Vib. 294, 410–417.
Jung, D., Chung, J., 2008. In-plane and out-of-plane motions of an extensible semi-circular pipe conveying fluid. J. Sound Vib. 311, 408–420.
Kuznetsov, Y.A., Kuznetsov, I.A., Kuznetsov, Y., 1998. Elements of Applied Bifurcation Theory. Springer.
Łuczko, J., Czerwiński, A., 2017. Nonlinear three-dimensional dynamics of flexible pipes conveying fluids. J. Fluid Struct. 70, 235–260.
Łuczko, J., Czerwiński, A., 2019. Three-dimensional dynamics of curved pipes conveying fluid. J. Fluid Struct. 91, 102704.
Luo, Y., Tang, M., Ni, Q., Wang, Y., Wang, L., 2016. Nonlinear vibration of a loosely supported curved pipe conveying pulsating fluid under principal parametric resonance. Acta Mech. Solida Sin. 29, 468–478.
Misra, A.K., Païdoussis, M.P., Van, K.S., 1988a. On the dynamics of curved pipes transporting fluid Part II: extensible theory. J. Fluid Struct. 2, 245–261.
Misra, A.K., Païdoussis, M.P., Van, K.S., 1988b. On the dynamics of curved pipes transporting fluid. Part I: inextensible theory. J. Fluid Struct. 2, 221–244.
Nakamura, K., Yamashita, K., Taniguchi, A., Yoshizawa, M., 2009. Nonlinear out-of-plane vibration of a curved pipe due to pulsating flow. In: ASME 2009 International Design Engineering Technical Conferences and Computers and Information in Engineering Conference, pp. 1679–1686.
Ni, Q., Tang, M., Wang, Y., Wang, L., 2013. In-plane and out-of-plane dynamics of a curved pipe conveying pulsating fluid. Nonlinear Dynam. 75, 603–619.
Païdoussis, M.P., 1998. Fluid-structure Interactions: Slender Structures and Axial Flow. Academic press.
Païdoussis, M.P., Li, G.X., 1993. Pipes conveying fluid: a model dynamical problem. J. Fluid Struct. 7, 137–204.
Païdoussis, M.P., Semler, C., 1993. Nonlinear dynamics of a fluid-conveying cantilevered pipe with an intermediate spring support. J. Fluid Struct. 7, 269–298.
Schilder, F., Dankowicz, H., Li, M., 2020-03-22. Continuation Core and Toolboxes (COCO). SourceForge (Accessed: 2022-09-22). https://sourceforge.net/projects/cocotools.
Shabana, A.A., 1996. An Absolute Nodal Coordinate Formulation for the Large Rotation and Deformation Analysis of Flexible Bodies. Technical Report, Department of Mechanical Engineering, University of Illinois at Chicago.
Tang, S., Sweetman, B., 2021. A geometrically-exact momentum-based nonlinear theory for pipes conveying fluid. J. Fluid Struct. 100, 103190.
Tang, Y., Wang, G., Ding, Q., 2022. Nonlinear fractional-order dynamic stability of fluid-conveying pipes constituted by the viscoelastic materials with time-dependent velocity. Acta Mech. Solida Sin. 1–13. https://doi.org/10.1007/s10338-022-00328-1.
Tüfekçi, E., Arpaci, A., 1998. Exact solution of in-plane vibrations of circular arches with account taken of axial extension, transverse shear and rotatory inertia effects. J. Sound Vib. 209, 845–856.
Yamashita, K., Nakamura, K., Yabuno, H., 2010. Out-of-Plane vibration of a curved pipe due to pulsating flow (nonlinear interactions between in-plane and out-of-plane vibrations). In: ASME 2010 3rd Joint US-European Fluids Engineering Summer Meeting Collocated with 8th International Conference on Nanochannels, Microchannels, and Minichannels, pp. 1197–1207.
Ye, S.-Q., Ding, H., Wei, S., Ji, J.-C., Chen, L.-Q., 2021. Non-trivial equilibriums and natural frequencies of a slightly curved pipe conveying supercritical fluid. Ocean Eng. 227, 108899.
Yun-dong, L., Ze-gang, S., 2021. Analysis of planar motion for curved pipe conveying fluid with different types of initial configuration. J. Vib. Eng. Technol. 1–16.
Zhou, K., Ni, Q., Chen, W., Dai, H., Peng, Z., Wang, L., 2021a. New insight into the stability and dynamics of fluid-conveying supported pipes with small geometric imperfections. Appl. Math. Mech. 42, 703–720.
Zhou, K., Ni, Q., Chen, W., Dai, H.L., Hagedorn, P., Wang, L., 2021b. Static equilibrium configuration and nonlinear dynamics of slightly curved cantilevered pipe conveying fluid. J. Sound Vib. 490, 115711.
Zhu, B., Chen, X.-C., Guo, Y., Li, Y.-H., 2021. Static and dynamic characteristics of the post-buckling of fluid-conveying porous functionally graded pipes with geometric imperfections. Int. J. Mech. Sci. 189, 105947.